Bivariate uncertainty analysis for impact testing

2007 Meas. Sci. Technol. 18 3565

(http://iopscience.iop.org/0957-0233/18/11/041)

Meas. Sci. Technol. **18** (2007) 3565–3571 doi:10.1088/0957-0233/18/11/041

Bivariate uncertainty analysis for impact testing

H S Kim and T L Schmitz

University of Florida, Department of Mechanical and Aerospace Engineering, Gainesville, FL 32611, USA

E-mail: hyosoo94@ufl.edu

Received 19 June 2007, in final form 22 August 2007
Published 4 October 2007
Online at stacks.iop.org/MST/18/3565

Abstract
This paper evaluates uncertainty contributors for frequency response function (FRF) measurements obtained through impact testing. The FRF is an important estimator for the structural dynamics of tool-holder–spindle-machine assemblies and is used as an input to analyses of milling dynamics. Therefore, it is of interest to determine the confidence in the measurement results. In this work, we present a bivariate uncertainty analysis that considers statistical variations, imperfect calibration coefficients for the hammer and transducer, misalignment between the intended and actual force direction during impact and mass loading (when using an accelerometer). The complex-valued FRF can be expressed by its real and imaginary parts, which are potentially correlated. This correlation is included in the bivariate analysis. An ellipsoid-shaped confidence region (at each frequency) is defined in the complex plane; the size and orientation of this region is determined from the individual input uncertainties. The scalar, total uncertainty is then determined using an eigen analysis of the FRF covariance matrix. Experimental results are provided.

Keywords: uncertainty, frequency response function, bivariate, ellipsoid, cosine error, mass loading

(Some figures in this article are in colour only in the electronic version)

1. Introduction

In this paper, we identify and combine primary uncertainty contributors for tool point frequency response function (FRF) measurements completed using impact testing[1]. By impacting the free end of the tool-holder–spindle-machine assembly with an instrumented hammer, a wide range of frequencies can be excited simultaneously. The resulting response is typically recorded using a low mass accelerometer, although non-contact transducers can also be applied. The time domain responses are (Fourier) transformed into the frequency domain and the complex ratio of the vibration response to the input force is calculated to determine the assembly FRF. We focus on impact testing because it is the most common method used to quickly identify the tool point FRF required for milling process dynamics analyses (see, e.g., review papers [1, 2]).

The paper is organized as follows. First, a statistical analysis of multiple impacts is completed where the bivariate nature of the complex data is respected using a multivariate uncertainty analysis technique. Next, the transducer calibration coefficient uncertainty is considered. Then, the cosine error caused by the incorrect force application direction and the mass loading introduced by the accelerometer are explored, including the bias correction in both cases. (The reader may note that this paper does not address system-dependent sampling, filtering or windowing issues and assumes that the voltage outputs by the transducers represent accurate estimates of the tool point dynamics, except for the uncertainty sources identified here.) After the individual uncertainty contributors are identified and analyzed, a discussion of their relative influences is presented. This discussion is followed by conclusions regarding this study.

[1] Our application of interest is tool point FRFs. However, impact testing is applied in many other situations requiring structural dynamics information as well.

2. Statistical uncertainty

In this section, we explore the statistical variation of multiple, single impact FRFs obtained from tests performed on a 19.1 mm diameter carbide rod inserted in a shrink fit tool holder, which was clamped in an HSK-63A high-speed spindle. Because the FRF is a complex-valued (or bivariate) function, an ellipsoidal uncertainty region with a 95% level of confidence is identified at each frequency, rather than the more traditional single-dimensional confidence interval. The ellipsoidal region is defined by [3]

$$(\bar{x}-\mu)^{\mathrm{T}}V^{-1}(\bar{x}-\mu) \leqslant \frac{(n-1)p}{n-p}F_{\alpha;p,(n-p)}, \tag{1}$$

where $\bar{x}$ is the vector of frequency-dependent mean values of the real and imaginary components of the sample FRFs; μ are the outer points of the confidence region that define the ellipsoidal boundary (when the equality is satisfied); V is the covariance matrix; n is the number of samples; $F_{\alpha;p,(n-p)}$ is the statistic of the F distribution with p, $(n-p)$ degrees of freedom; for a probability $(1-\alpha)$, α is the level of significance ($\alpha = 0.05$ for 95% confidence); and p is the number of variates ($p = 2$ for the complex FRF).

As shown in equation (1), the covariance matrix, which includes the standard variances of the real and imaginary FRF components, as well as the estimated covariance between them, plays an important role in obtaining the ellipsoidal uncertainty region. The following steps are taken from the analysis detailed in [4] for constructing the covariance matrix. The mean values of the real and imaginary components are given by

$$\overline{\mathrm{Re(FRF)}} = \frac{1}{n}\sum_{i=1}^{n}\mathrm{Re(FRF}_i) \tag{2}$$

and

$$\overline{\mathrm{Im(FRF)}} = \frac{1}{n}\sum_{i=1}^{n}\mathrm{Im(FRF}_i). \tag{3}$$

The standard uncertainties of the real and imaginary components are determined from equations (4) and (5).

$$u(\mathrm{Re(FRF)}) = \sqrt{\frac{1}{n(n-1)}\sum_{i=1}^{n}[\mathrm{Re(FRF}_i) - \overline{\mathrm{Re(FRF)}}]^2} \tag{4}$$

$$u(\mathrm{Im(FRF)}) = \sqrt{\frac{1}{n(n-1)}\sum_{i=1}^{n}[\mathrm{Im(FRF}_i) - \overline{\mathrm{Im(FRF)}}]^2}. \tag{5}$$

The estimated covariance between Re(FRF) and Im(FRF) is calculated using equation (6).

$$u(\mathrm{Re(FRF)}, \mathrm{Im(FRF)}) = \frac{1}{n(n-1)}\sum_{i=1}^{n}[\mathrm{Re(FRF}_i) - \overline{\mathrm{Re(FRF)}}][\mathrm{Im(FRF}_i) - \overline{\mathrm{Im(FRF)}}]. \tag{6}$$

The covariance matrix is constructed by setting the on-diagonal terms of the (2×2) matrix equal to the standard variances of the real and imaginary components and the off-diagonal terms equal to the covariance between them. The covariance matrix is symmetric because $u(\mathrm{Re(FRF)}, \mathrm{Im(FRF)}) = u(\mathrm{Im(FRF)}, \mathrm{Re(FRF)})$.

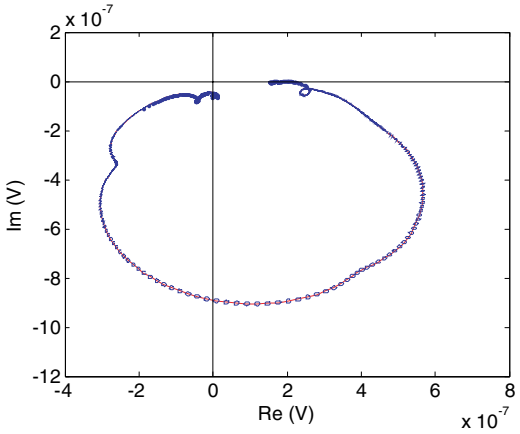

Figure 1. Mean FRF (uncalibrated) plotted in the complex plane. The ellipsoidal uncertainty regions (95% confidence level) from the statistical variation are shown at selected frequencies.

$$V = \begin{bmatrix} u^2(\mathrm{Re(FRF)}) & u(\mathrm{Re(FRF)}, \mathrm{Im(FRF)}) \\ u(\mathrm{Im(FRF)}, \mathrm{Re(FRF)}) & u^2(\mathrm{Im(FRF)}) \end{bmatrix}. \tag{7}$$

Note that each of the results in equations (1)–(7) are frequency dependent; a new value is defined for each frequency within the measurement range of interest. Figure 1 shows the mean FRF and the ellipsoidal uncertainty regions for 100 single impact tests carried out on the representative tool, where the data are displayed in the complex plane. The small ellipsoid size relative to the overall FRF scale indicates that the 100 impacts were quite repeatable (low statistical variation). The reader may note that these are the voltage data only. The calibration coefficients for the hammer and accelerometer are applied and their uncertainties treated in the following section.

3. Calibration coefficient uncertainty

In order to convert the measured voltages to appropriate engineering units, the transducer calibration coefficients must be applied. In this section, we combine the inherent uncertainty in these values with the statistical measurement variation shown in the previous section. The FRF is expressed in terms of the calibration coefficients, C_x and C_f, for the accelerometer (or other transducer) and hammer, respectively, and the corresponding voltages, V_x and V_f, by

$$\mathrm{FRF} = \frac{C_x V_x}{C_f V_f}. \tag{8}$$

For the accelerometer and hammer applied in this study, the manufacturers provided ranges of $\pm 1\%$ for C_x and $\pm 2.7\%$ for C_f. The standard uncertainties were estimated from these ranges by selecting an appropriate distribution. We assumed a uniform distribution with 100% confidence that the actual value falls within the specified range for both coefficients [5, 6]. See equations (9) and (10).

$$u(C_x) = \frac{0.01 \times C_x}{\sqrt{3}} \tag{9}$$

$$u(C_f) = \frac{0.027 \times C_x}{\sqrt{3}}. \tag{10}$$

Uncertainty in the calibration coefficients was included using a bivariate form of the Gaussian error propagation law for complex numbers [7]; a brief review of this method is now provided. We consider an arbitrary measurement function:

$$y = f(X) = f(x_1, x_2, \ldots, x_m) \tag{11}$$

that describes the relationship between a complex-valued quantity of interest, the measurand y, and m influence quantities, x_1 to x_m. The function f consists of two scalar functions, f_1 and f_2, that evaluate the real and imaginary components, respectively (i.e., $y = f_1(X) + f_2(X)$). The uncertainty in the values assigned to the input quantities is represented by a $(2m \times 2m)$ covariance matrix:

$$V(X) = \begin{bmatrix} u^2(x_{11}) & u(x_{11}, x_{21}) & \cdots & u(x_{11}, x_{1m}) & u(x_{11}, x_{2m}) \\ u(x_{21}, x_{11}) & u^2(x_{21}) & \cdots & u(x_{21}, x_{1m}) & u(x_{21}, x_{2m}) \\ \vdots & \vdots & \ddots & \vdots & \vdots \\ u(x_{1m}, x_{11}) & u(x_{1m}, x_{21}) & \cdots & u^2(x_{1m}) & u(x_{1m}, x_{2m}) \\ u(x_{2m}, x_{11}) & u(x_{2m}, x_{21}) & \cdots & u(x_{2m}, x_{1m}) & u^2(x_{2m}) \end{bmatrix}, \tag{12}$$

where the on-diagonal terms represent the standard variance of the associated inputs and the off-diagonal terms represent the covariance. Also, the first subscript for each term indicates the real (1) or imaginary part (2) of the selected input quantity, while the second subscript identifies the quantity in question (values of 1 to m). The uncertainty in the measurand y is expressed in a (2×2) covariance matrix:

$$V(y) = J(y)V(X)J(y)^{\mathrm{T}}, \tag{13}$$

where $J(y)$ is the $(2 \times 2m)$ Jacobian matrix of the partial derivatives of the scalar components of f with respect to the scalar elements of X as shown in equation (14).

$$J(y) = \begin{bmatrix} \frac{\partial f_1}{\partial x_{11}} & \frac{\partial f_1}{\partial x_{21}} & \frac{\partial f_1}{\partial x_{12}} & \frac{\partial f_1}{\partial x_{22}} & \cdots & \frac{\partial f_1}{\partial x_{1m}} & \frac{\partial f_1}{\partial x_{2m}} \\ \frac{\partial f_2}{\partial x_{11}} & \frac{\partial f_2}{\partial x_{21}} & \frac{\partial f_2}{\partial x_{12}} & \frac{\partial f_2}{\partial x_{22}} & \cdots & \frac{\partial f_2}{\partial x_{1m}} & \frac{\partial f_2}{\partial x_{2m}} \end{bmatrix}. \tag{14}$$

In [7], a convenient approach to obtain $J(y)$ is introduced. The Jacobian matrix is described using a (2×2) block structure that can be associated with the derivatives of f with respect to the individual bivariate inputs:

$$J(y) = [J_1(y)J_2(y)\cdots J_m(y)], \tag{15}$$

where

$$J_i(y) = \begin{bmatrix} \frac{\partial f_1}{\partial x_{1i}} & \frac{\partial f_1}{\partial x_{2i}} \\ \frac{\partial f_2}{\partial x_{1i}} & \frac{\partial f_2}{\partial x_{2i}} \end{bmatrix}. \tag{16}$$

These blocks represent the bivariate sensitivity coefficients for the analysis. They can be related directly to the complex partial derivatives of f by a matrix representation for complex numbers, $z = a + \mathrm{j}b$, where the mapping

$$M(z) = \begin{bmatrix} a & -b \\ b & a \end{bmatrix} \tag{17}$$

generates a (2×2) matrix representation for z. The full Jacobian matrix can then be written as

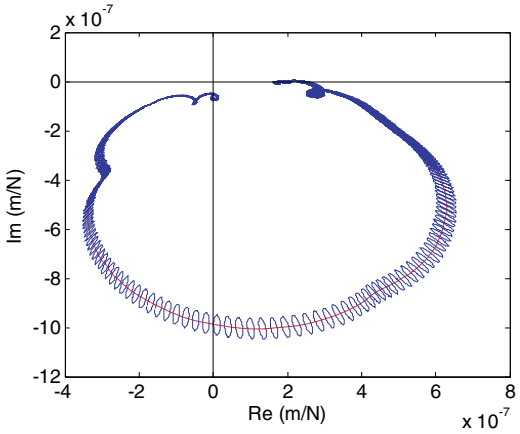

Figure 2. Ellipsoidal uncertainty regions including the statistical variation and calibration coefficient uncertainties. The mean FRF (calibrated) is also shown.

$$J(y) = \left[M\left(\frac{\partial f}{\partial x_1}\right) M\left(\frac{\partial f}{\partial x_2}\right) \cdots M\left(\frac{\partial f}{\partial x_m}\right) \right]. \tag{18}$$

For the calibration coefficient uncertainty propagation, three uncertain input variables in equation (8) were considered. Here, we have set the frequency domain voltage ratio V_x/V_f equal to V_r:

$$y = \mathrm{FRF} = f(V_r, C_x, C_f). \tag{19}$$

The first step was to construct the input covariance matrix, where the upper left (2×2) terms depend on the statistical evaluation of the measured (unscaled) FRFs and no correlation was considered between the real-valued accelerometer and hammer calibration coefficients.

$$V(V_r, C_x, C_f) = \begin{bmatrix} u^2(\mathrm{Re}(V_r)) & u(\mathrm{Re}(V_r), \mathrm{Im}(V_r)) & 0 & 0 & 0 \\ u(\mathrm{Im}(V_r), \mathrm{Re}(V_r)) & u^2(\mathrm{Im}(V_r)) & 0 & 0 & 0 \\ 0 & 0 & u^2(\mathrm{Re}(C_x)) & 0 & 0 \\ 0 & 0 & 0 & 0 & 0 \\ 0 & 0 & 0 & u^2(\mathrm{Re}(C_f)) & 0 \\ 0 & 0 & 0 & 0 & 0 \end{bmatrix} \tag{20}$$

Next, the Jacobian matrix was determined using

$$J(\mathrm{FRF}) = \left[M\left(\frac{\partial \mathrm{FRF}}{\partial V_r}\right) M\left(\frac{\partial \mathrm{FRF}}{\partial C_x}\right) M\left(\frac{\partial \mathrm{FRF}}{\partial C_f}\right) \right]. \tag{21}$$

The output covariance matrix was computed using equation (13). Finally, the ellipsoidal uncertainty region was defined using equation (1) as shown in figure 2. It is seen in figure 2 that the frequency-dependent ellipsoidal regions have expanded substantially with respect to figure 1. This suggests that calibration coefficient uncertainty is a more important contributor than the statistical variation to the overall measurement uncertainty. Figure 3 shows the ellipsoidal regions near the maximum real part of the FRF. The inclination of the ellipse major axis relative to the Re and Im axes indicates

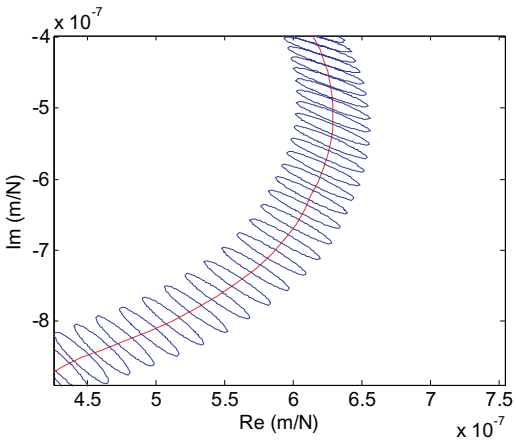

Figure 3. Section of the ellipsoidal uncertainty regions shown in figure 2. The non-vertical/horizontal inclination of the major axes of the ellipses indicates correlation between the real and imaginary parts of the FRF.

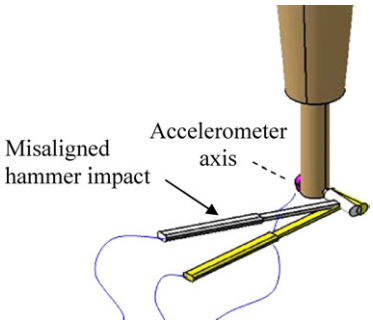

Figure 4. Schematic of the misalignment between the hammer impact direction and accelerometer (transducer) axis which leads to the cosine error.

correlation between the real and imaginary components of the FRF in this frequency range. At the limit, a horizontal or vertical major axis of an ellipse represents no correlation while a 45° line (i.e., the ellipse has collapsed to a line) denotes the perfect correlation. The reader may note the variation in the orientation of the ellipse between figure 1 and figure 2. Even through the calibration factors are real valued and uncorrelated, they still serve to change the resulting correlation (ellipse orientation) after propagation through equation (13).

4. Cosine uncertainty

During impact tests, the force input direction is generally not perfectly aligned with the sensor direction. This leads to the well-known cosine error, as well as the subsequent bias. As shown in figure 4, any misalignment between the force and sensor directions causes the force which actually excites the system to be less than the force sensed by the hammer load cell (in the extreme, striking the tool in a direction perpendicular to the vibration transducer axis would lead to zero excitation in the absence of mechanical cross-talk, but the hammer load cell would still observe the full force level).

To evaluate typical force direction misalignment angles, tests were performed on a cutting force dynamometer by three users. Impacts were completed in the three Cartesian directions as shown in figure 5. The misalignment angle, β, between the actual and intended directions for the dynamometer tests was calculated from the dot product of the norms of the force along the selected axis and the resultant force. Figure 6 and equation (22) depict the x direction case, where F_x is the dynamometer force and F_h is the hammer load cell force. The means of the misaligned angles for each direction by the three testers are provided in table 1.

Table 1. Mean misalignment angles for x, y and z directions from three testers.

Direction	β (deg) for tester 1	β (deg) for tester 2	β (deg) for tester 3	Mean β (deg)
x	2.7	3.8	2.5	3
y	1.8	1.9	3.7	2.5
z	1.1	2.8	6.6	3.5

$$\beta = \cos^{-1}\left(\frac{F_x F_h}{|F_x||F_h|}\right). \tag{22}$$

Due to the angular misalignment, the FRF amplitude is under estimated (biased). The true FRF, FRF_t, should be determined from the force component in the transducer direction, F_t. However, the measured FRF, FRF_h, is actually computed using the force reported by the hammer load cell. See equation (23). The bias correction is realized using equation (24) [5], where $u(\beta)$ is the standard uncertainty in the misalignment angle. Here we have assumed a standard uncertainty equal to the mean value of 3.0° from table 1. Figure 7 shows the magnitude of the measured and corrected FRFs. The bias correction is clearly quite small. This reveals that, while input force direction can vary in impact testing, under typical conditions it is not a primary error source.

$$\text{FRF}_t = \frac{X}{F_t} \qquad \text{FRF}_h = \frac{X}{F_h} \tag{23}$$

$$\text{FRF}_t = \frac{X}{F_t} = \frac{X}{F_h\left(1 - \frac{1}{2}u^2(\beta)\right)} = \text{FRF}_h\left(1 - \frac{1}{2}u^2(\beta)\right)^{-1}. \tag{24}$$

Since the misalignment angle is not perfectly known, uncertainty propagation can be performed using the Gaussian uncertainty propagation law. The measurand expression was obtained by replacing F_t in the denominator of the FRF_t equation with $F_h\cos(\beta)$. The bivariate error propagation was then carried out on two input variables: the measured FRF, including both calibration coefficient and statistical uncertainty, and the misalignment angle,

$$\text{FRF}_t = f(\text{FRF}_h, \beta). \tag{25}$$

The same steps described in the previous section were again followed. First, the input covariance matrix was written as

$$V(\text{FRF}_h, \beta) = \begin{bmatrix} u^2(\text{Re}(\text{FRF}_h)) & u(\text{Re}(\text{FRF}_h), \text{Im}(\text{FRF}_h)) \\ u(\text{Im}(\text{FRF}_h), \text{Re}(\text{FRF}_h)) & u^2(\text{Im}(\text{FRF}_h)) \\ 0 & 0 \\ 0 & 0 \end{bmatrix} \begin{bmatrix} 0 & 0 \\ 0 & 0 \\ u^2(\text{Re}(\beta)) & 0 \\ 0 & 0 \end{bmatrix}. \tag{26}$$

Figure 5. Photographs of setups for impact tests on the cutting force dynamometer in the (*a*) *x*, (*b*) *y* and (*c*) *z* directions.

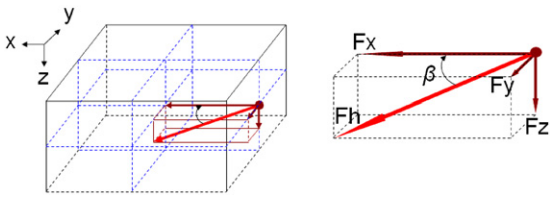

Figure 6. Angular misalignment between the dynamometer *x*-axis and the hammer impact direction.

Next, the Jacobian matrix was described by

$$J(\mathrm{FRF}_t) = \left[M \left(\frac{\partial \mathrm{FRF}_t}{\partial \mathrm{FRF}_h} \right) M \left(\frac{\partial \mathrm{FRF}_t}{\partial \beta} \right) \right]. \tag{27}$$

Finally, the output covariance matrix was computed using equation (13) and the ellipsoidal uncertainty region was defined using equation (1). The results are shown in figure 8. The similarity to figure 2 shows that cosine error is not a significant uncertainty contributor in this case.

5. Mass loading uncertainty

Because the tool point dynamics are modified when attaching the accelerometer to the structure, the influence of the accelerometer mass must be considered. To correct the mass loading bias, we applied equation (28) [8], where m_a is the accelerometer mass (0.93 mg with range of ±1%); A_i indicates accelerance, or the complex ratio of acceleration to input force; and the c and m subscripts denote corrected and measured values, respectively. Even though the bias is removed using this approach, uncertainty remains in the corrected result. Again, the ellipsoidal uncertainty region was established using the Gaussian uncertainty propagation law. To carry out the analysis, we converted the accelerance terms in equation (28) to receptances (or the complex displacement to force ratios) using $A_i = -\omega^2 R_i$, where ω is the frequency (in rad s^{-1}) and R_i is the receptance. See equation (29).

$$A_c = \frac{A_m}{1 - m_a A_m} \tag{28}$$

$$R_c = \frac{R_m}{1 + m_a \omega^2 R_m}. \tag{29}$$

Note that the measured response in equation (29) is actually the corrected response from the cosine error analysis, which includes the uncertainties due to the measurement statistical variation and calibration coefficients. The input variables to the propagation law were R_m (or FRF_t, the corrected response from cosine error) and m_a.

$$R_c = f(\mathrm{FRF}_t, m_a). \tag{30}$$

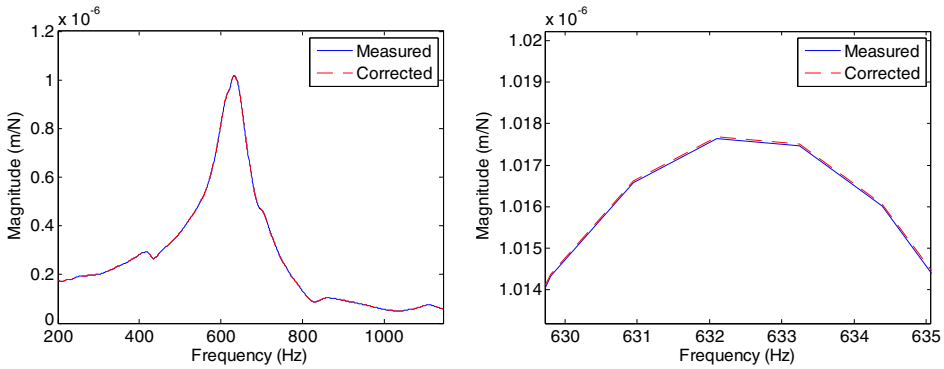

Figure 7. Cosine error bias correction. Left: measured and corrected FRFs. Right: it is seen that the cosine error bias leads to an underestimated magnitude, but the effect is small.

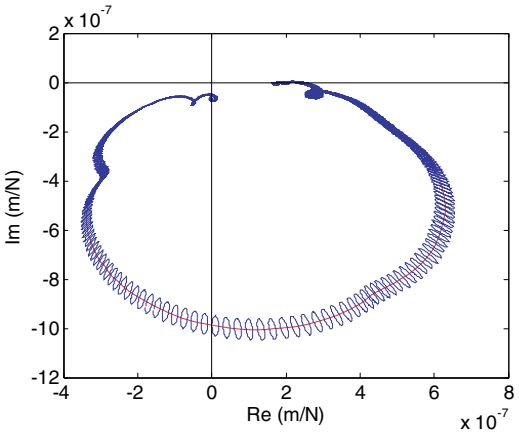

Figure 8. Ellipsoidal uncertainty regions including statistical, calibration coefficient and cosine uncertainties. The mean FRF is also shown.

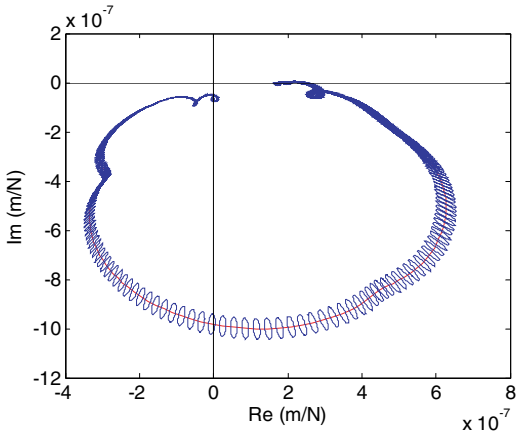

Figure 9. Ellipsoidal uncertainty regions including statistical, calibration coefficient, cosine and mass loading uncertainties. The mean FRF is also shown.

The input covariance matrix was given by

$$V(\mathrm{FRF}_t, m_a) = \begin{bmatrix} u^2(\mathrm{Re}(\mathrm{FRF}_t)) & u(\mathrm{Re}(\mathrm{FRF}_t), \mathrm{Im}(\mathrm{FRF}_t)) \\ u(\mathrm{Im}(\mathrm{FRF}_t), \mathrm{Re}(\mathrm{FRF}_t)) & u^2(\mathrm{Im}(\mathrm{FRF}_t)) \\ 0 & 0 \\ 0 & 0 \end{bmatrix} \begin{bmatrix} 0 & 0 \\ 0 & 0 \\ u^2(\mathrm{Re}(m_a)) & 0 \\ 0 & 0 \end{bmatrix}. \tag{31}$$

The Jacobian matrix was

$$J(R_c) = \left[M\left(\frac{\partial R_c}{\partial \mathrm{FRF}_t}\right) M\left(\frac{\partial R_c}{\partial m_a}\right) \right] \tag{32}$$

and the same steps were again followed to identify the final frequency-dependent ellipsoidal uncertainty regions. See figure 9; the similarity to figure 8 suggests that the contribution is not significant for mass loading uncertainty in this case.

6. Discussion

Although figures 1, 2, 8 and 9 correctly represent the frequency-dependent, ellipsoidal confidence regions for the measured system, they are difficult to compare quantitatively. In order to directly compare the relative influence of each of the four uncertainty contributors considered in this paper, we have applied the notion of the scalar 'total variance' discussed by Hall in [7]. As noted, the orientation and size of each elliptical uncertainty region can be geometrically interpreted using an eigen analysis of the measurand covariance matrix. The eigenvectors of this matrix (at the selected frequency) represent the major and minor axes of the ellipse, while the eigenvalues represent the associated (uncorrelated) variances. The sum of the eigenvalues can then be taken as a measure of the 'total variance' and used to quantify the frequency-dependent contributions of the individual uncertainty terms in a scalar sense. Figure 10 shows the per cent contribution of each uncertainty source relative to the FRF magnitude as a function of frequency. It is seen that the cosine and mass loading uncertainties are negligible with respect to the calibration coefficient and statistical uncertainties and that the overall uncertainty is at approximately the 2% level. Additionally,

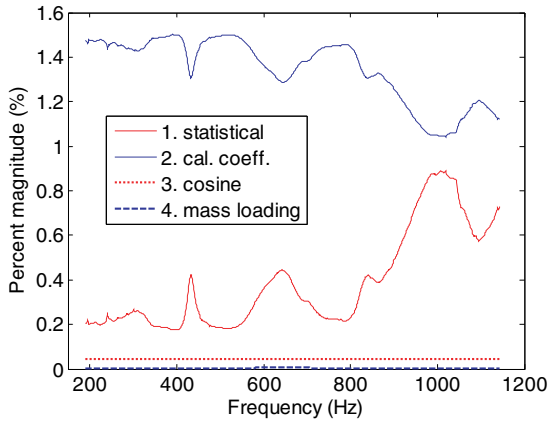

Figure 10. Per cent total uncertainty relative to the FRF magnitude as a function of frequency. It is seen that the calibration coefficients are the primary uncertainty contributor, although the statistical variation becomes more significant at higher frequencies.

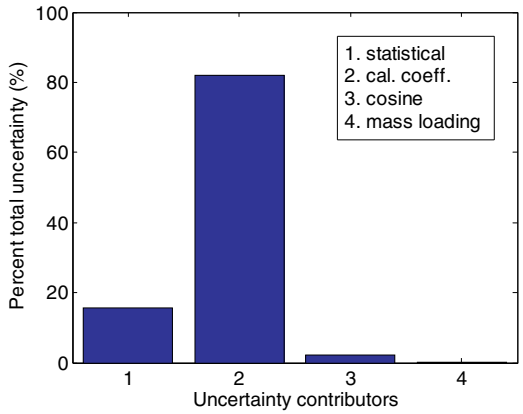

Figure 11. Per cent total uncertainty for four contributors. It is shown that the calibration coefficients dominate the total uncertainty.

it is observed that the statistical uncertainty tends to grow with frequency, which makes sense given that the hammer impact occurs over a non-zero, finite interval and leads to an excitation bandwidth with decreasing energy at higher frequencies. The relative contributions over the full bandwidth of interest were determined by summing the uncertainty for each contributor over all frequencies and then normalizing to the total uncertainty for all contributors. These results are shown on a percentage basis in figure 11 where it is seen that the calibration coefficients comprise $>80\%$ of the total uncertainty for this study.

7. Summary

In this work, we evaluated uncertainty contributors for FRF measurements obtained using impact testing. We presented a bivariate uncertainty analysis that considered statistical measurement variations, imperfect calibration coefficients for the hammer and transducer, misalignment between the intended and actual force direction during impact and mass loading (when using an accelerometer). An ellipsoidal confidence region at each frequency within the bandwidth of interest was defined in the complex plane. Additionally, the biases introduced by the misalignment between the hammer and vibration transducer axes and accelerometer mass loading were corrected. Finally, a scalar representation of the ellipsoidal confidence regions was shown and calibration coefficients were identified as the primary uncertainty contributor for the tests completed as part of this study.

Acknowledgments

This work was supported by the National Science Foundation through grant numbers DMI-0555645 and DMI-0238019 (G Hazelrigg). Any opinions, findings, and conclusions or recommendations expressed in this material are those of the authors and do not necessarily reflect the views of the National Science Foundation. Additional partial financial support for Mr Kim was provided by the Korea Science and Engineering Foundation through grant number D00010. The authors also wish to acknowledge helpful discussions with Dr T Schultz.

References

[1] Smith S and Tlusty J 1991 An overview of modeling and simulation of the milling process *ASME J. Eng. Ind.* **113** 169–75
[2] Altintas Y and Weck M 2004 Chatter stability of metal cutting and grinding *Ann. CIRP* **53** 619–42
[3] Jobson J D 1992 *Applied Multivariate Data Analysis* (NJ: Springer)
[4] Ridler N M and Salter M J 2002 An approach to the treatment of uncertainty in complex *s*-parameter measurements *Metrologia* **39** 295–302
[5] International Standards Organization (ISO) 1993 *Guide to the Expression of Uncertainty in Measurement* (corrected and reprinted 1995)
[6] Taylor B N and Kuyatt C E 1994 Guidelines for evaluating and expressing the uncertainty of NIST measurement results *NIST Technical Note* **1297** 1994 edition
[7] Hall B D 2004 On the propagation of uncertainty in complex-valued quantities *Metrologia* **41** 173–7
[8] Ashory M 1999 High quality modal testing methods *PhD Dissertation* Imperial College of Science, Technology and Medicine, London